THE STRUCTURE AND EVOLUTION OF LOCBURST: THE BATSE BURST LOCATION ALGORITHM

GEOFFREY N. PENDLETON, MICHAEL S. BRIGGS, R. MARC KIPPEN, WILLIAM. S. PACIESAS, MARK STOLLBERG, AND
PETE WOODS
Department of Physics, University of Alabama in Huntsville, Huntsville, AL 35899

CHARLES A. MEEGAN AND GERALD J. FISHMAN
NASA/Marshall Space Flight Center, Huntsville, AL 35812

MIKE L. MCCOLLOUGH
USRA NASA/MSFC, Huntsville, AL 35812

AND

VALERIE CONNAUGHTON
NRC NASA/MSFC, Huntsville, AL 35812

Received 1997 November 13; accepted 1998 September 3

ABSTRACT

The gamma-ray burst (GRB) location algorithm used to produce the BATSE GRB locations is described. The general flow of control of the current location algorithm is presented, and the significant properties of the various physical inputs required are identified. The development of the burst location algorithm during the releases of the BATSE 1B, 2B, and 3B GRB catalogs is presented so that the reasons for the differences in the positions and error estimates between the catalogs can be understood. In particular, differences between the 2B and 3B locations are discussed for events that have moved significantly and the reasons for the changes explained. The locations of bursts located independently by the interplanetary network (IPN) are used to illustrate the effect on burst location accuracy of various components of the algorithm. IPN data and locations from other gamma-ray instruments are used to calculate estimates of the systematic errors on BATSE burst locations.

Subject headings: gamma rays: bursts — methods: numerical

1. INTRODUCTION

We describe here the burst location algorithm, LOCBURST, used for gamma-ray bursts (GRBs) and other short-lived transient sources observed by the Burst and Transient Source Experiment (BATSE; Fishman et al. 1989). This is the algorithm used by the BATSE instrument team to produce the final locations for the GRB catalogs. The validity of the isotropy measurement for the GRB population observed by BATSE rests on the accuracy and reliability of this algorithm. In addition, the measurement limitations affecting BATSE's sensitivity to burst repetition and clustering are defined by LOCBURST as well. Therefore, a detailed description of the algorithm is valuable for those interested in evaluating these burst properties with the BATSE burst data.

The algorithm employs a series of location procedures that produce successively more accurate locations and location error estimates. Its performance is continuously evaluated, and the importance of specific systematic errors is identified by analyzing in-flight data. As a result, the algorithm design has been improved between successive BATSE burst catalog releases and the accuracy of certain physical inputs enhanced to reduce the effects of the more prominent systematic errors.

This work is organized into sections containing analyses and descriptions relevant to particular aspects of LOCBURST. In § 2 we define the physical inputs required and outline the general structure of the current LOCBURST algorithm. This overview is necessary to properly define the complexity of the optimization problem and to understand why the algorithm development proceeded as it has. In § 3 we discuss the evolution of the LOCBURST code between successive catalog releases so that the reasons for the differ-ences between the 1B, 2B, and 3B BATSE burst catalogs can be understood. In § 4 we present estimates of the instrument's systematic errors using comparisons with other instruments and transient event types. In § 5 we highlight those aspects of the LOCBURST algorithm and its development that are not common to general gamma-ray instruments and data analysis systems. We summarize, at a general level, the issues that have made the optimization of the BATSE location algorithm a complicated and time-consuming project and describe our planned future efforts to increase the scientific output of the BATSE burst location procedure.

2. BURST LOCATION WITH BATSE

At first glance, the method for locating bursts with the BATSE Large Area Detectors (LADs) seems fairly simple. There are eight 2025 cm^2 LADs arranged on the *Compton Gamma Ray Observatory* (*CGRO*) spacecraft with their faces parallel to those of an octahedron, and, to first order, they exhibit a cosine-like response in their effective area as a function of the source viewing angle. In the absence of any other effects, the relative rates in three of these detectors viewing a burst simultaneously can be used to uniquely identify the burst's direction in the sky. Therefore, a simple inversion using the rates in the three detectors most brightly illuminated by the burst might be expected to produce the burst's intensity and the two angles defining the burst location. In practice, however, a more elaborate model of the instrument and its environment is necessary to obtain accurate burst locations with BATSE.

LOCBURST employs a nonlinear χ^2 minimization algorithm that fits modeled count rates to observed count rates to obtain the final location. The algorithm finds the

optimum values for the independent variables of interest: two angles that specify the burst's location, the burst intensity averaged over the source interval selected, and a power-law index for a first-order representation of the burst's spectrum in the energy range where the fitting is taking place. Particular values of these independent variables are convolved through a model of the instrument response, including atmospheric scattering effects, and compared using a χ^2 calculation to the background-subtracted count rates separated into distinct energy channels for each detector viewing the burst. Rates of change in χ^2 are calculated with respect to the independent burst variables and are used to find the χ^2 minimum with conventional minimization procedures.

The procedure described above applies to the determination of a location when the parameters representing the instrument response and atmospheric scattering are held fixed. The optimization of the location algorithm's accuracy is an entirely different problem, in which the accuracy of the instrument response and atmospheric scattering parameters are enhanced, and even the structure of the algorithm itself is modified. This optimization procedure is considerably more involved than one might expect.

To appreciate the potential complexity of the instrument and atmospheric scattering parameter model, it is useful to consider the number of independent instrument parameters involved. Three attributes can be used to describe the behavior of the BATSE LAD response: the incident photon energy, the photon energy deposited in the detector, and the angle between the incident photon and the detector normal, or source viewing angle. The disklike geometry of an LAD makes its projected effective area a strong function of the source viewing angle. When photons enter the detector crystal and interact, they may deposit all or part of their energy so that there is a distribution of measured energy depositions in an LAD for an ensemble of monoenergetic incident photons. The shape of these energy deposition distributions and the dependence of the detector effective area on-source viewing angle are both strong functions of the incident photon energy. These detector properties are described in more detail below. Although there are minor variations in some of these properties between the eight LADs, for the purpose of a conservative summary of independent variables affecting LOCBURST, we will consider only the three properties listed above.

In addition to the physics of the interaction of gamma rays in the detectors, the LAD response is also characterized by the particular characteristics of the readout electronics, and the dependence of the Na I efficiency for converting energy deposition to scintillation photons on the total energy deposition. A channel-to-energy conversion algorithm, derived from calibration data, describes a mapping of photon energy deposition (not necessarily the total photon energy, as mentioned above) to instrument channel number. Also, a dead-time correction estimates the amount of time that the instrument is inactive and unable to respond to gamma rays while the electronics are processing an event, typically several microseconds per event. The percentage of dead time increases as the flux increases. We will consider these factors as independent for each detector, adding 16 instrument parameters to our list. Furthermore, background subtraction must be performed independently for each detector, adding another eight parameters.

Atmospheric scattering is one of the more complicated phenomena that significantly affects BATSE burst location. It is characterized by the photon energy incident on the Earth's atmosphere, the recoil energy of the photon scattered from the atmosphere into the detector, the elevation of the GRB source direction above the Earth's horizon, and the polar and azimuthal angles of the atmospherically scattered photons, for a total of five independent variables necessary to describe atmospheric scattering.

In the representation presented above, the instrument response can be described by 33 independent parameters, which poses what appears to be far too multidimensional a problem to actually solve. Simply optimizing the instrument parameter set using a set of known interplanetary network (IPN) locations in a neural net training approach would not have been reliable because of the vast domain spanned by both the instrument parameters and the GRB independent variable set, as well as potential correlations between the two. Furthermore, the algorithmic structure of LOCBURST itself evolved significantly during the optimization process in a manner that would not be reproducible with neural net training. The approach we have found to be effective for this problem is to compartmentalize the parameters into self-similar sets (i.e., those parameters related to atmospheric scattering in one set) and then study the effect of each set of parameters on the GRB location accuracy. This is an iterative process that is data-analysis intensive and relies heavily on the use of ground-based calibration and in-flight data to evaluate the impact of each response characteristic. The goal is not to completely specify the response characteristics and their impact with virtually infinite precision, but rather to map out the domain of location accuracy dependence that each response characteristic inhabits and then to enhance the accuracy of the most important ones, in keeping with what is practically achievable. We will describe in some detail below the sets of response characteristics that are most important for BATSE burst locations and then outline the current algorithm.

The detector response of the BATSE LADs has been extensively modeled with detailed Monte Carlo simulations optimized with calibration data. The details of this effort are described elsewhere (Pendleton et al. 1995a); however, some of the detector characteristics most relevant to burst location are described here.

Figure 1 shows the total detector response in units of effective area as a function of incident photon energy for a source along the detector axis. This total response curve includes events that have deposited their full energy in the detector as well as those that have deposited only a fraction of their energy. The solid horizontal line at 2025 cm^2 is the total geometric area of the LAD Na I crystal. The effective area remains below 85% of the geometric area at lower energies because the charged particle detector directly in front of the LAD absorbs the photons before they can get to the LAD detector crystal. At higher energies the thinness (1.27 cm) of the crystal reduces the photon conversion efficiency and increases the frequency of partial energy deposition by the photons that do convert.

The detector response is maximum in the nominal BATSE trigger energy range of 50–300 keV (shown in Fig. 1, *vertical dashed lines*). Burst spectra are often quite hard out to 1 MeV or more, so their observed counts spectra are distributed with high significance over this entire energy
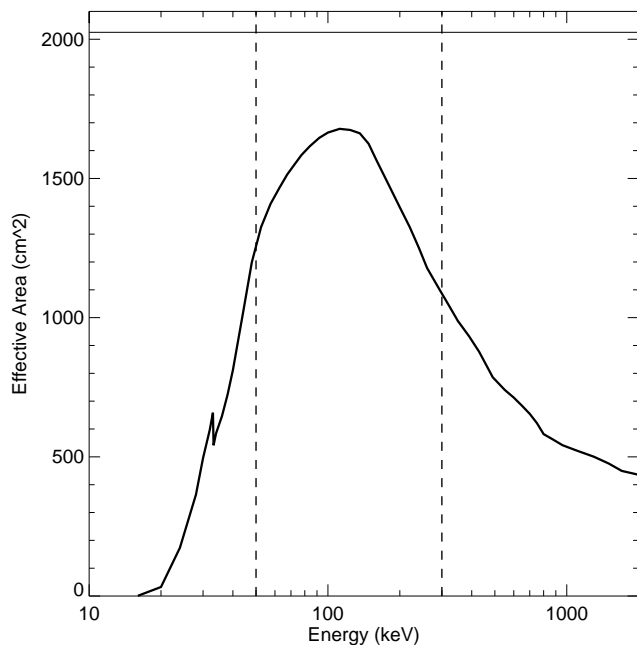
range and often well beyond 300 keV. Since bursts have significant counts over this energy range, centered on the response maximum, we select this interval in order to minimize the effects of uncertainties in the channel-to-energy conversion algorithm and hence the actual position of the vertical dashed lines in Figure 1. If the energy boundaries of this interval are shifted upward or downward slightly, the changes in detector response at either end of the interval work to cancel each other out. In contrast, if we selected the 20–30 keV range, a small shift upward or downward in the energy boundaries would produce a larger change in the response integrated over the interval. The interval selection above is designed to minimize the effects of systematic errors in the channel-to-energy conversion model. The stability of the channel-to-energy conversion for the LADs is maintained using an automatic gain control algorithm in the flight software that keeps the position of the 511 keV background line fixed in channel space with about 1% accuracy. In addition, the accuracy of the Monte Carlo modeling is not as strongly affected by the details of the instrument and spacecraft geometry in the 50–300 keV range as it is at significantly higher and lower energies. Therefore, the detector response as a function of the source viewing angle is least likely to be affected by systematic errors in this energy range. Finally, the BATSE burst data generally yields the best signal-to-noise ratio in this energy range, due to both the hardness burst spectra and the specific characteristics of the LAD detector response.

A less beneficial consequence of the bursts' hard spectra is that the detector response above 300 keV is important for those photons that undergo partial energy deposition in the LAD detector crystal.

The response in counts for an LAD in the energy range 50–300 keV as a function of the source viewing angle is shown in Figure 2 for a number of different incident photon energies. The lowest curve on the plot represents the
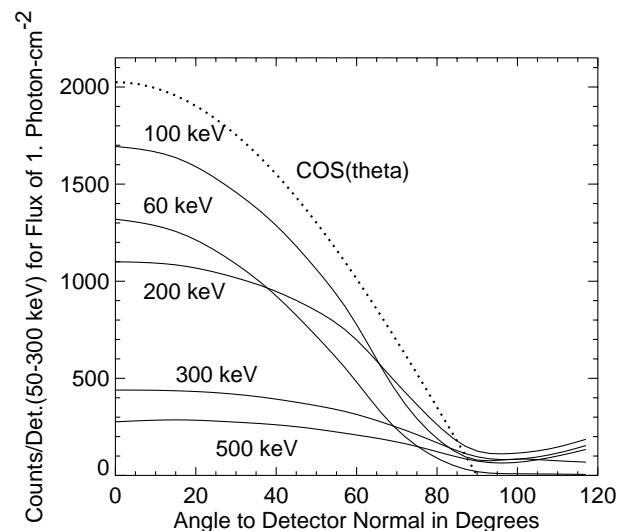
response for 500 keV photons in the 50–300 keV counts range used for burst location, effectively excluding photons that deposit all 500 keV of their energy in the detector. The partial energy deposition angular response of the 500 Kev photons is much flatter than a cosine response (*dotted line*). The full energy deposition peaks of the 100 and 200 keV photon curves, by contrast, are contained within the 50–300 keV range. In general, the detector angular response is more cosine-like at lower energies and flatter as a function of angle at higher energies. The striking changes in angular response as a function of energy demonstrates the need for first-order spectral modeling, at least across the trigger energy range.

Experience with relatively steady sources, such as SN 1987A, observed with modified LADs from a balloon platform (Pendleton et al. 1995b) predisposes us to regard background subtraction as a likely candidate for systematic error. However, GRBs are relatively short and intense events compared with other gamma-ray sources, so it is possible to pick background intervals quite close to the burst interval. This minimizes the most troublesome aspect of background systematics for BATSE, which is that the background changes with time in ways that are difficult to predict. The most important aspects of the background subtraction procedure for LOCBURST are the selection of the background intervals as close to the source interval as possible and selection of a source interval that maximizes the signal-to-noise ratio.

In order to ensure that the optimum source and background intervals can be selected, the LOCBURST software is required to work with virtually all the BATSE LAD data types. For the most part, the 16 energy channel continuous data or the four channel discriminator data with 2.048 and 1.024 s resolution, respectively, are used. Background intervals, generally within 50 s or so of the actual burst interval are selected, and the background is modeled with a linear or quadratic form. The linear background model form is quite sufficient in almost all cases for the purposes of burst location, because we are using relatively high time-resolution data in intervals close to the burst emission interval in an energy range where the background is well behaved. We

explore the potential impact of background systematics in more detail below.

Of all the properties of GRB detection, atmospheric scattering requires the most detailed modeling. A fully three-dimensional modeling of the atmospheric scattering convolved through the detector response is required to significantly reduce the systematic error on burst locations. In the next section we will show that it is the incremental improvements in the implementation of the scattering model in the location algorithm that have been primarily responsible for the reduction in the systematic error between successive BATSE burst catalog releases. Directly below we will present data illustrating the relative intensity of the atmospheric scattering effect and the strength of its dependence on the orientation of BATSE relative to the Earth and the burst elevation above the horizon.

The atmospheric scattering data were generated with the EGS electromagnetic cascade Monte Carle code in the energy range 10–5 MeV using a spherical geometry of concentric shells representing an atmosphere with exponential density. The scattered source flux is convolved through the appropriate detector response in order to produce the scattered source counts observed by each detector. In Figure 3 distributions of the ratio of the scattered flux to the direct flux are shown for the detectors used in 1650 burst locations. Here direct flux refers to the measured burst flux incident directly on the detector, and scattered flux refers to the burst flux that is scattered off the Earth and then measured by the detector. The histograms are in units of number of bursts per histogram bin.

The distributions are separated by the detector-to-burst viewing angle where "first" refers to the detector with the smallest viewing angle, generally the brightest detector, and "sixth" refers to the detector with the largest viewing angle, generally the weakest detector. In the 3B catalog LOC-BURST algorithm it was possible to select either four or six detectors for a burst location. The reasons why this option was included will be described in the next section. In the brightest detector, the scattering rate rarely exceeds 10%; however, in the third brightest detector, the most commonly observed scattering rate is between 20% and 50%. In the fourth through sixth brightest detectors, the scattered rate often exceeds the direct rate. The somewhat surprisingly high amplitude of the observed scattering has a significant impact on burst location accuracy.

The fidelity required of the atmospheric scattering representation is significantly increased by its strong dependence on the assumed source direction. In Figure 4 the scattered/direct ratio is plotted to demonstrate its dependence on three important source viewing angles. The ratios are plotted versus the source elevation, i.e., the angle between the direction to the geocenter and the direction to the GRB. The data are grouped into sets with specific ranges of the detector normal to geocenter angle and detector normal to burst location angle (Fig. 4, "Geo" and "Det," respectively). The data in the left-most column of panels are for downward-facing detectors, whereas those in the right-most column are for sky-facing detectors. Similarly, the top row is for detectors facing the burst, and the bottom row is for detectors at larger angles to the burst.

As one would expect, the downward-facing detectors see more Earth-scattered flux than the upward-facing detectors. Furthermore, the ratio of scattered/direct flux is larger for detectors with larger burst viewing angles. It also is clear
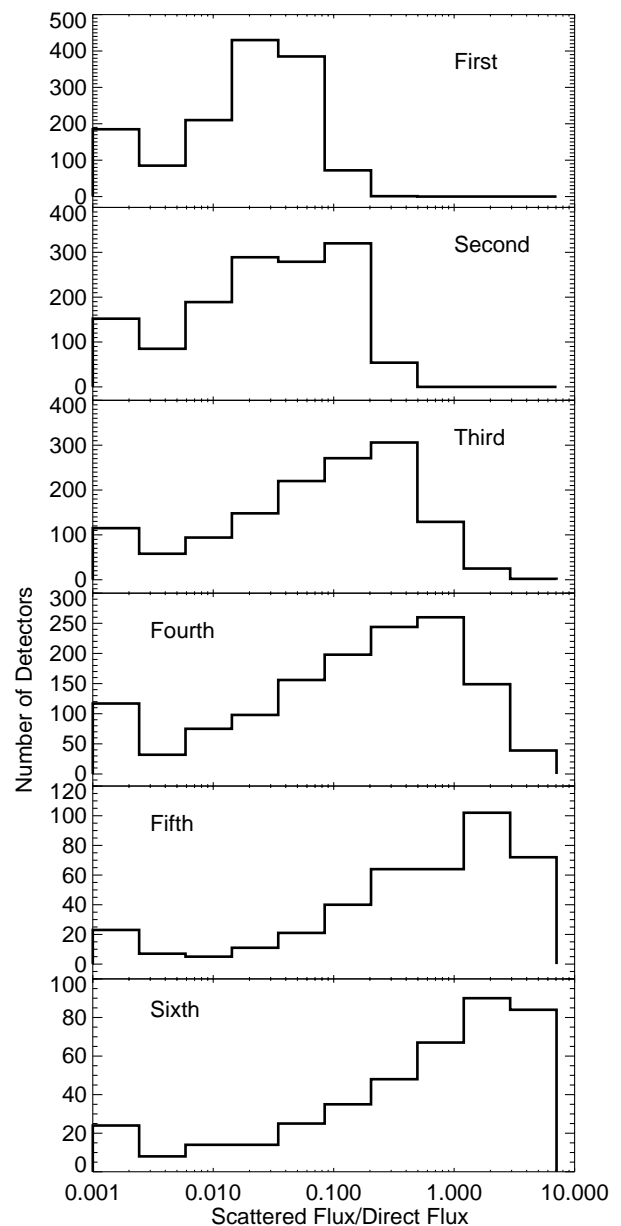

FIG. 3.—Distributions of ratios of atmospherically scattered flux to direct flux in the 50–300 keV energy range for the first through sixth brightest LAD detectors used by LOCBURST for the burst locations.

from these plots that this ratio can change substantially over a source elevation range of only a few degrees, particularly for downward-facing detectors viewing the source at larger angles. This rapid rate of change in the scattered flux with source elevation, a parameter that changes during the burst location process, requires that the scattering model be accessed by LOCBURST with precision as a function of source elevation.

The detector response parameters described above are the most relevant for GRB location with BATSE. The size of the systematic error on the BATSE burst locations is directly related to the accuracy with which each of these characteristics is represented. Obviously, several of these parameters have complex multidimensional structure and are intimately coupled together. The practical optimization of this set of response parameters for burst location required a balanced synthesis of human and cybernetic
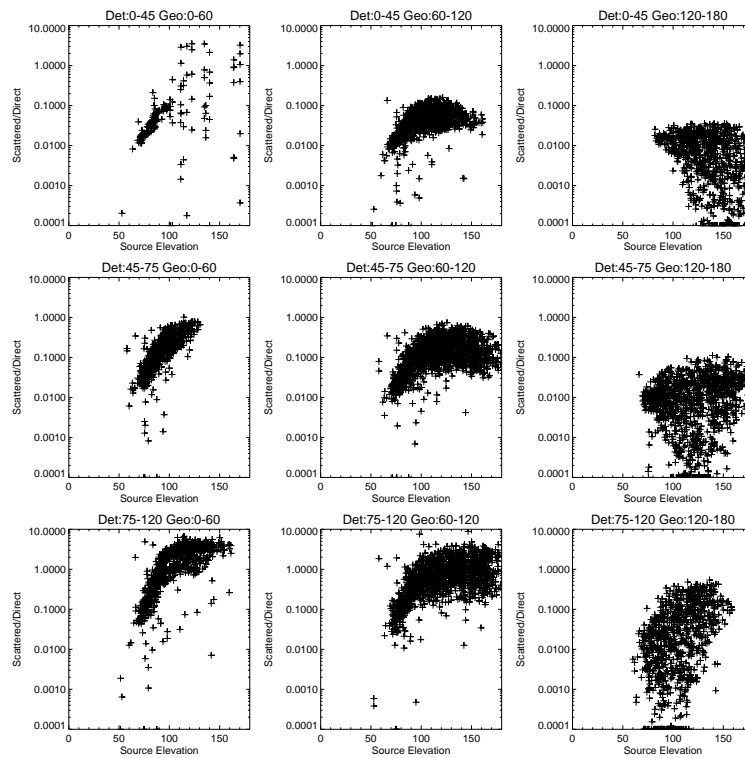
FIG. 4.—Ratio of atmospherically scattered flux to direct flux as a function of source elevation, detector normal to geocenter angle, and burst viewing angle.

analytic capabilities and repeated testing with flight data. The LOCBURST algorithm is described in detail below. The optimization of the algorithm itself required the same powerful and flexible approach as the optimization of the instrument parameter set.

The location software employs three algorithms with increasing levels of accuracy and complexity that are run consecutively to produce the final burst location. After the location has been calculated, a fourth algorithm uses a grid search to verify that a χ^2 minimum has been found and to calculate the location error contours.

Figure 5 uses 12 IPN (Hurley et al. 1996) located bursts, 24 bursts located by COMPTEL (Kippen et al. 1998), and two located by WATCH (Gorosabel et al. 1996), for a total of 38, to demonstrate the accuracy of the three consecutive algorithms in LOCBURST. Bursts such as these that have been well located by other spacecraft will be referred to hereafter as independently located bursts (ILBs). The same set of bursts is used for each of the three histograms in this figure.

The thickest histogram shows the accuracy of the first-order algorithm in the form of an integral distribution of IPN-to-BATSE location separations. In this algorithm the brightest three of the eight detectors are selected. A power-law spectral form is applied across the energy range used, and the detector response as a function of source angle is calculated for each of the three selected detectors. The calculated detector response is combined with the observed rates to solve for the burst location consistent with these three detectors. This preliminary calculation is a simple numerical solution for the burst direction and intensity based on the count rates in the three brightest detectors and the detector angular response, in contrast to the full nonlinear χ^2 minimization technique used to produce the final

location. At this point we have a crude first-order location where atmospheric scattering has not been taken into account.

The second step is to take this crude location and use it to estimate the atmospheric scattering observed in all eight detectors. After that, if data with 16 channel energy resolution is used, the power-law spectral index is optimized
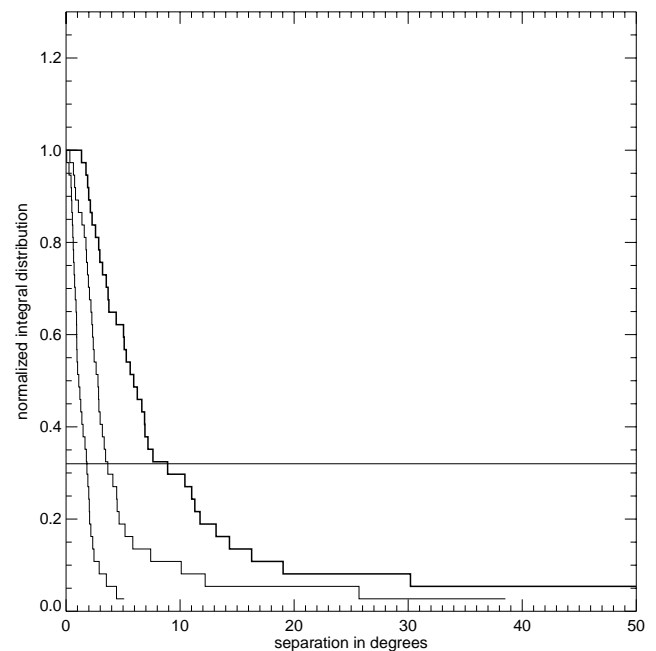

FIG. 5.—LOCBURST location accuracy for the three consecutive algorithms as determined by absolute offset from bursts located using other spacecraft.

using a χ^2 minimization routine. Finally, the eight burst source rates are examined again after having their estimated atmospheric scattering removed, and the three brightest detectors are selected again. This entire procedure is repeated until consecutive iterations change the location by less than $1°$, producing our second-order location. The accuracy of this algorithm is shown as the histogram with a line of medium thickness in Figure 5. The addition of atmospheric scattering reduces the systematic error by about a factor of 2.

The third algorithm uses a χ^2 minimization technique that produces our best estimate of the burst location. The preliminary location calculated in the second level is used as input for a χ^2 minimization routine. Either the brightest four or the brightest six detectors are selected for this calculation using a procedure described in detail later in the text. In this algorithm, the modeled direct and scattered count rates are compared with the observed source count rates, and the difference between the model and the data is used to calculate χ^2. This algorithm also calculates the derivative of the modeled rates with respect to azimuth and elevation angles in *CGRO* coordinates, and these derivatives are used in a conventional χ^2 minimization routine to find the χ^2 minimum. The spectral index and intensity are allowed to vary as well, although in practice these values rarely change significantly from those obtained by the preliminary algorithm. The χ^2 minimum was chosen when χ^2 changed by less than 0.1 three times. The thin-lined histogram in Figure 5 shows the accuracy of this algorithm that produces the final LOCBURST output for the burst catalog. The accuracy of these locations has improved by a factor of 2 relative to the second-order locations.

After the minimization has completed, a χ^2 grid search is performed about the final location that verifies that the burst location is at the global χ^2 minimum and also calculates the statistical error contours. The grid search uses 121 points arranged in a two-dimensional square pattern centered about the minimum location, with the grid points spaced at the larger of the $1°0$ or the statistical error estimate. This procedure maps out the χ^2 contours around the minimum, which can deviate significantly from concentric circles, as will be shown below.

3. THE DEVELOPMENT OF THE LOCATION ALGORITHM

The LOCBURST algorithm was improved significantly between the 1B and 3B BATSE burst catalog releases. To first order, the improvements of the total LOCBURST algorithm accuracy between successive versions of LOCBURST closely parallels the accuracy of the individual nested algorithms in the 3B version, as is displayed in Figure 5.

This similarity emphasizes an important property of the optimization process. In a particular version of the location algorithm there is generally one dominant source of systematic error. If this systematic error is not corrected, then neither improvements in other instrument parameters nor the addition of more sophisticated algorithms will significantly reduce the location systematic error. It is necessary to remove the sources of systematic error sequentially, like the layers of an onion, so each can be properly identified and remedied. For example, the pre-1B locations did not use a particularly accurate representation for the atmospheric scattering. As a result, the χ^2 minimization algorithm did not improve the locations significantly compared

with the second-level algorithm. Once a better scattering model was implemented, the χ^2 minimization algorithm produced more accurate locations. These improvements included a better physical model of the scattering, as well as a more accurate methods of implementing it. Once the more important response parameters, like scattering, had been optimized, then improvements in other instrument parameters and refinements to the algorithm could be tested. The LOCBURST optimization procedure is described in detail below.

Before the BATSE 1B burst catalog was produced, our estimate of the RMS systematic error on the burst locations produced by LOCBURST was about $7°$ (Brock et al. 1992). The entire LOCBURST algorithm at this point consisted of the three detector iterative procedures and the χ^2 minimization procedure, where only four detectors could be used at any one time. The detector response was calculated only to $90°$. If, during the course of χ^2 minimization, the location moved so that the members of the set of four brightest detectors actually changed, then the value of χ^2 could jump discontinuously. This somewhat objectionable attribute was left in place during our initial LOCBURST optimization efforts so we could focus on refining the instrument parameters. The atmospheric scattering was estimated by a numerical algorithm that calculated the flux of photons scattered by a single scattering interaction in a planar representation of the Earth's atmosphere.

Our extensive Monte Carlo simulations of atmospheric scattering (Pendleton et al. 1992), primarily being developed for spectroscopy software, showed that the majority of the photons undergo more than one scattering before leaving the atmosphere, and the single scattering approximation was not sufficiently accurate for the purposes of LOCBURST. A database of atmospheric scattering rates convolved through the detector response functions, optimized for high-speed access, was developed for LOCBURST.

An extensive investigation of solar flares was performed to study the effects of angular response and the channel-to-energy conversion on the location accuracy (Pendleton et al. 1994). Solar flares are bright events that are relatively soft compared with GRBs and also come from a known location. Their softness makes the amount of atmospheric scattering they suffer rather small compared with bursts and increases their sensitivity to the channel-to-energy calibration. The LAD angular response at large angles and low energies was adjusted as a result of this study. These corrections were incorporated into the detector response matrices. The full atmospheric scattering correction was applied to the flares and found to have a noticeable effect on their model count rates.

After developing software tools to implement the fully developed atmospheric scattering correction and the detector response matrix calibrations into LOCBURST, we formed the Burst Location Optimization Team, tasked with identifying and correcting sources of systematic error in LOCBURST. We identified five most probable areas where systematic errors could affect the accuracy of LOCBURST: detector angular response, atmospheric scattering, background subtraction, channel-to-energy conversion, and dead-time correction. The evaluation of the systematic error for any particular realization of LOCBURST requires the analysis of an ensemble of sources with known locations. We wanted to test versions of LOCBURST with calibration corrections turned on and off, and applied in various com-

binations in order to determine the importance of each one. This meant analyzing relatively large ensembles of solar flares and a set of 12 IPN-located bursts repeatedly. Therefore, we developed a batch mode of analysis for LOC-BURST so our test group of bursts and solar flares could be analyzed as the potential sources of systematic error were explored.

When we explored the effects of uncertainties on the channel-to-energy conversion algorithm, we found that the locations of solar flares were quite sensitive to it, and bursts were not. At the time we were conducting in-flight calibrations with Crab occultation data (Pendleton et al. 1994) in order to characterize the range of uncertainty in the channel-to-energy conversion and to map out nonlinearites in the readout electronics for spectroscopy purposes. We explored the possible range uncertainty in the channel-to-energy conversion by implementing distinct realizations of the algorithm in LOCBURST and testing it on our ensemble of bursts and flares.

The location accuracy of the flares was significantly affected by these variations. Because solar flares are soft, most of the significance was in the data bin with the lowest energy range that, for 16 channel data, is approximately 55–70 keV. Therefore, the solar flare location was quite sensitive to variations in the low-energy edge for this bin between detectors. These variations changed the model of both the absolute rate in each detector and the shape of the angular response in that bin. For bursts, however, the dependence was not evident. When we varied the channel-to-energy implementation between events, the location accuracy of our 12 IPN events did not vary significantly. When we examined the distribution of counts in the 50–300 keV energy range for bursts, we found them to be much more uniformly distributed in energy than the solar flare counts, a situation that one would expect, since bursts are so much harder than flares. The result of this broad distribution in counts is that the detector angular response for bursts is more representative of an average of the response across the entire 50–300 keV energy range. Therefore, selecting this broad energy range for GRB localization minimizes the effect of channel-to-energy conversion uncertainties.

Studies of dead-time effects on burst location uncertainty (Horack et al. 1993) showed that at the highest rates, inaccuracies in the dead-time correction caused errors in the relative rates between the detectors viewing the burst from different angles. This type of error, of course, directly affects locations. In practice, it is usually possible to select intervals in very bright bursts where the emission is not too intense to calculate the dead time accurately yet still have enough source counts so that the statistical error is less than 1°.

As was stated earlier, we were predisposed to consider background subtraction inaccuracies as a likely source of systematic error because of our previous experience with nonburst sources. As a result, we invested considerable effort into investigating how the accuracy of source and background interval selection and background fitting affected the burst location accuracy. Using our batch processing algorithm, we studied various source and background interval selection criteria and different orders of the polynomial fit of the background as a function of time. We found that the linear background model was sufficient, and selecting source intervals that maximized the signal-to-noise ratio minimized the statistical error without increas-

ing the systematic error. The one constraint was that intervals that contained overly bright flux had to be omitted to avoid dead-time distortions.

The results of these studies that produced the greatest improvement in burst locations were summarized at the first Compton symposium (Brock et al. 1993). The two areas where algorithmic improvements were most effective were the improved atmospheric scattering correction and the angular response correction. The implementation of these corrections reduced the RMS systematic error from 7° to 4°. At this stage, the algorithm was frozen and used to produce the 1B catalog. The χ^2 minimization still used only four detectors, and the algorithm was run in batch mode with the source and background intervals input from a preselected list.

Since our location algorithm calibration studies were ongoing at the time of the 2B BATSE catalog release, these bursts were produced with the same version of LOC-BURST used to produce the 1B data. We believed at the time that adding the gradient of the atmospheric scattering to the χ^2 minimization would improve the accuracy of our final locations. The complexity of the scattering representation made this a relatively time-consuming procedure, and significant effort was involved in optimizing the algorithm's run time. We had also identified several cases where, near the χ^2 minimum, the four brightest detectors changed. In this case, as the location moved, one detector would see the burst at greater than 90° and be dropped, and another detector would see the burst at less than 90° and be added. This caused the total χ^2 value to change discontinuously. There were even a few cases where the location algorithm toggled back and fourth across one of these boundaries in an endless loop. Clearly, this situation had to be remedied, and the most obvious way to do this was to extend the detector response beyond 90°.

Figure 2 shows that the response used in LOCBURST has been extended in this way. The basic procedures used to build the DRMs (Pendleton et al. 1995) were employed to combine calibration data and Monte Carlo simulations to extend the response functions to 145°. The software will nominally calculate the response to 180°, but we believe that substantial azimuthal variations on the response will become present beyond 145°. The simulations were performed using a detailed model of the BATSE detector and the *CGRO* spacecraft. Beyond 145° to the detector normal, large, massive spacecraft components eclipse the detectors in complicated patterns as a function of source direction. Modeling this would require an extensive effort that is not necessary. Instead, we developed the four or six detector selection option.

Figure 6 illustrates the BATSE source viewing conditions that distinguish cases where either four or six detectors are selected. We represent the BATSE geometry with an octahedron where its faces are parallel with the surfaces of the BATSE LADs. Figure 6a shows a case where a burst illuminates four detectors equally on one side of the spacecraft. This is the simplest of four detector cases. Figure 6b shows a case where burst flux is coming straight along the normal to the brightest detector and illuminates the second through fourth brightest detectors equally. In contrast to these two scenarios, Figure 6c shows the cases where a burst illuminates two detectors equally brightly and barely illuminates the surrounding four detectors. It can be difficult to distinguish between the three configurations shown in Figure
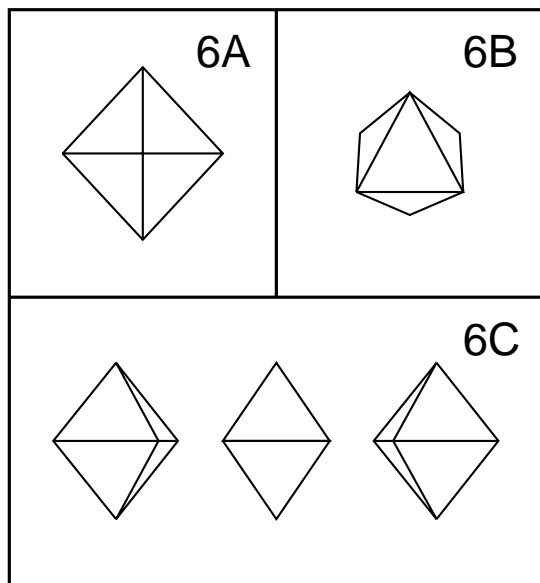
FIG. 6.—Schematic views of four and six detector location cases

FIG. 8.—Mirror point contour point for six detector location contour plot for trigger 1473.

6c, and limiting the algorithm to only four detectors causes the detector subset selection problem described above.

There is an additional complication introduced by atmospheric scattering that manifested itself in trigger 1473, which was also located by WATCH and the IPN (Gorosabel et al. 1996; Hurley et al. 1996). In Figure 4 we showed that the amplitude of the atmospherically scattered flux observed by BATSE increases strongly as the source position rises above the Earth's horizon, i.e., as the source elevation increases. This trend, coupled with the source viewing geometry shown in Figure 6c, can produce two distinct local χ^2 minima locations, one of which is in the wrong place on the sky. Figure 7 illustrates this difficulty. A source at a relatively high elevation can produce a strong atmospherically scattered signal in an Earth-facing detector that it does not directly illuminate. If we begin our location estimate without atmospheric scattering, then the predicted source location will have a considerably lower elevation angle. That location, being nearer the Earth's horizon, will not predict very much scattering. Therefore, the location algorithm will tend to minimize about this lower elevation location. Using six instead of four detectors provides enough information to resolve this problem.

Figure 8 shows the χ^2 contours for burst 1473. There are two separate local χ^2 minima that are typical of the ambi-
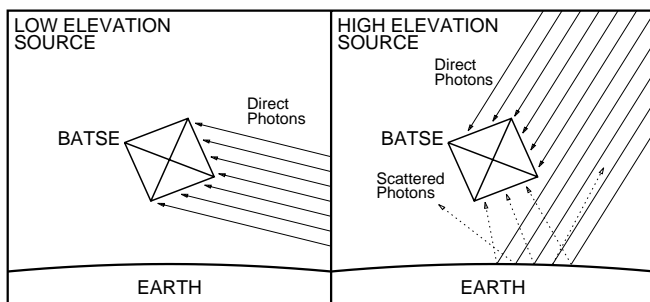
guity diagrammed in Figure 6. When six detectors are used, the χ^2 minimum value at the correct source location is significantly lower than that at the false minimum; in the case of 1473, it is 4 times lower at the true location.

The procedure for implementing the six detector option is for the burst processor to observe the background subtracted rates at the end of the three detector iterative procedure with the atmospheric scattering rate estimates removed. At that time, if the two brightest detectors have rates within 30% of each other and are generally 3 times brighter than the surrounding four detectors, then the six detector option is selected. To ensure that the correct χ^2 minimum is found, the χ^2 minimum is calculated using the location from the three detector iterative procedure. Then a mirror point is selected that is on the opposite side of the two brightest detectors from the first χ^2 minimum. Mirror point locations would be equivalent to the two outer octahedron views in Figure 6c. The low-elevation and high-elevation source locations in Figure 7 are also mirror points.

The minimization procedure is run using this mirror point as an initial guess, and if a χ^2 minimum is found that is different from the first χ^2 minimum, then the location with the smallest χ^2 minimum value is selected as the true burst location. This is the procedure used to locate trigger 1473 that improved the location relative to the WATCH location by more than 15°. Use of six detectors does not always add enough information to force the location algorithm to exhibit only a single local χ^2 minimum, but it adds enough discriminating power to indicate which minimum produces a significantly better fit in almost all the cases encountered to date. An exception to this is trigger 1468, where it is difficult to tell which minimum is better. This relatively rare ambiguity is currently under study.

Figure 9 shows the angular separations between IPN (Hurley et al. 1996) and LOCBURST locations for bursts located using the six detector option. The histograms display the preliminary, intermediate, and final location separations in the same fashion as in Figure 5. However, we have added an additional thick, dashed histogram showing the final angular separations for these bursts using the four detector option instead of the appropriate six detector option. The use of the six detector option produces a noticeable improvement only for the final χ^2 minimization procedure and does not yield significant improvement for the

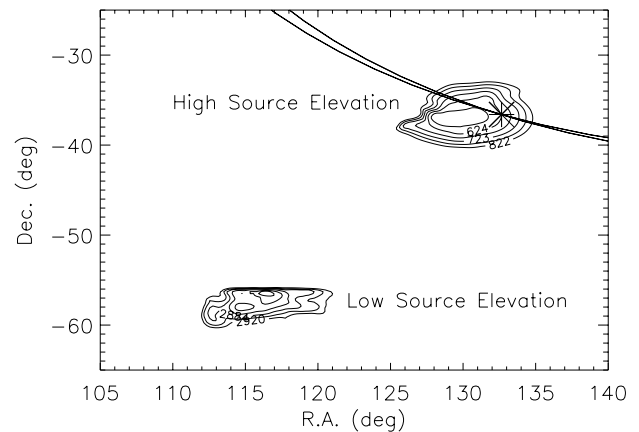FIG. 7.—Schematic of atmospheric scattering requiring the mirror point check for six detector locations.
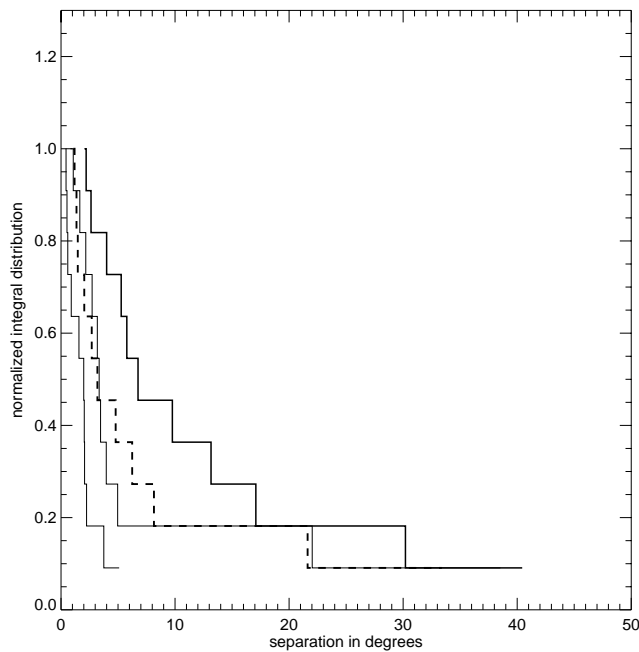
FIG. 9.—Locations for bursts emphasizing difference between four and six detector location accuracies for six detector geometry cases.

first- and second-order locations, except in a few extreme cases like trigger 1473. However, the method does improve the final locations significantly. The six detector option applied to four detector cases does not produce any improvement and can worsen the locations in some cases. Therefore, it is only applied when the location meets the criterion specified above. About 25% of the bursts in the 3B catalog were located using six detectors. One exception to this rule may be bursts located with four detectors where one of the four detectors views the burst at greater than 90° at the final calculated location. Initial studies indicate that it would be better to rerun these bursts with the six detector option.

In the 3B algorithm we implemented full modeling of the atmospheric scattering in the χ^2 grid search procedure. In this procedure, 121 points are sampled from a square grid centered on the χ^2 minimum location, with points spaced in spacecraft azimuth and elevation by the greater of $1°$ or the calculated 1σ statistical error. The response characteristics, including atmospheric scattering, are recalculated at each point, and χ^2 minimum is calculated. The resulting grid is used to build our χ^2 contour maps, which will be discussed in more detail below. In a few rare cases of complicated χ^2 contours, a χ^2 value is found during the grid search that is smaller than the one arrived at by the minimization procedure. When this happens, this new location is input to the χ^2 minimization routine, and the minimization and grid search procedures are run anew. The algorithm as described here has converged to a final location for all the BATSE bursts analyzed to date.

We also implemented the capability of crudely modeling broken power-law spectral forms in LOCBURST. Normally, a single power-law form is used because of its robustness in the analysis of weaker bursts. Since we are often restricted to the use of four channel data for short bursts or bursts with incomplete data coverage, the spectral model was one with three power-law indices joined at spectral

break points fixed in energy. For the four channel case this allowed the algorithm to solve for three spectral indices and an overall spectral amplitude.

The addition of this capability improved the value of the reduced χ^2 at the χ^2 minimum by ~ 2 but did not significantly affect the statistical or systematic error significantly except in a few special cases. The general improvement in χ^2 is expected, since we know bursts exhibit spectral curvature in the 50–300 keV range. It is somewhat surprising that this improvement in reduced χ^2 did not have a more noticeable affect on the size of the systematic error of most bursts.

The systematic error was improved for bursts where the actual spectral form of the burst was a very hard power law, a value of 1.0 or less, in the 50–300 keV range, and a significantly softer power law, a value of 2.5 or greater, above 300 keV. In these cases a single power-law fit with hard index of 1.3 or less would predict a much larger amount of atmospheric scattering than was actually present. Also, the apparent strength of the higher energy direct detector response down in the 50–300 keV energy range was significantly overrepresented. In this case, the spectral curvature option allowed for a more accurate representation of the instrument response.

The drawback of the current implementation of spectral curvature in LOCBURST is that it is unstable for weaker bursts—the majority of bursts. It tends to produce obviously erroneous fits to the weaker burst data (for example, a set of consecutive spectral indices from low to higher energy of -9, $+4$, -9). Consequently, the curvature option was exercised only for brighter bursts with indices harder than 1.3, which is less than 5% of the total population.

As we stated above, the 1B and 2B catalog source and background intervals were accessed from an automated batch data file. This is not the best approach for optimizing the signal-to-noise ratio for the burst source counts. Allowing an interactive processor to observe the rates from the selection of source and background intervals ensures that background subtraction does not cause obvious systematic errors. In fact, as we discuss below, there were cases where the less carefully monitored batch source and background selection process introduced significant systematic errors between the pre-1B locations and the 1B and 2B catalogs.

In the pre-3B location algorithms, both preburst and postburst background intervals were required. This caused problems for bursts where suitable preburst and postburst background intervals were not available because of telemetry gaps. The 3B algorithm allows for the selection of either pre- or postburst background intervals in isolation or together, as well as allowing for more combinations of distinct data types so the background selection can be as accurate as possible and the source's signal-to-noise ratio can be optimized. The combination of greater flexibility in the data-type selection and the careful interval selection resulted in a better signal-to-noise ratio for the source counts in the 3B analysis. As was shown above, the statistical error on the burst location is inversely proportional to the source flux signal-to-noise. The average statistical error for the 1B bursts was $5°.7$, compared with $4°.7$ for the same set of bursts in the 3B catalog.

The source counts are generally selected from an interval that yields a high level of signal-to-noise for the source counts values in each detector. However, in the 3B catalog analysis, intervals with source count rates that are too high, above 50,000 counts s^{-1}, are avoided because of inaccu-

racies in the LAD dead time correction at higher rates. Since the dead time is different for the separate detectors, inaccuracies in the correction can distort the relative rates in each detector. For example, the location of burst 143 obtained with the brightest intervals of the burst flux can be $9°$ away from the IPN location. Locations performed using data from source intervals more than 40 s after the burst trigger, with count rates below 50,000 counts s^{-1}, produce locations within $2°$ of the IPN location.

The topics listed in this section include the most important features and milestones in the evolution of LOC-BURST. In the next section we discuss the specific changes between the 2B and 3B final locations.

4. DIFFERENCES BETWEEN THE BATSE 2B AND 3B CATALOG LOCATIONS

During the implementation of the algorithm modifications described above, a set of 12 IPN located bursts, available at the time of the release of the 1B catalog, were used to assess the sensitivity of the burst location systematic errors to the fidelity of particular instrument parameter representations and algorithmic techniques. These were BATSE triggers 105, 109, 130, 143, 219, 249, 451, 999, 1025, 1085, 1121, and 1473. Since we had a large domain of instrument parameters and algorithmic approaches, and a relatively small test data set of IPN bursts, it was not possible to optimize the instrument parameter set by a purely empirical relaxation procedure. Each instrument parameter, as described above, had to have its accuracy refined using calibration information independent of the GRB locations.

Two bursts from this test set, triggers 1085 and 1473, were exceptional examples of the superiority of the six detector minimization option. Trigger 143 was an excellent example, demonstrating how selection of source intervals with count rates below 50,000 counts s^{-1} removed dead-time systematics. Analysis of these 12 bursts ensured that the algorithm was implemented without significant errors.

When the 3B catalog was produced (Meegan et al. 1996), all the bursts, including those previously analyzed and distributed with the 1B and 2B algorithms, were analyzed with the 3B software and procedure. About 12% of the 3B burst locations had moved by $20°$ or more relative to their 2B locations. All of these bursts were examined individually in detail to determine the reason why they moved. More than 75% of these bursts have 3B statistical errors greater than $5°$. These bursts generally had even larger 2B statistical errors. About 45% (6% of the total population) had improved locations due to improvements in the background interval selection procedure, described above. Another 50% of these bursts were more effectively located by the six detector option. This is checked by comparing the pre-3B modeled rates in the four detectors used with the source data rates and noting that the 3B catalog six detector analysis yields much better agreement between the model and the data than the older four detector case. Improvements in the atmospheric scattering implementation play a role here as well.

A few bursts in the 2B catalog were converted from Gamma Ray Observatory (GRO) to equatorial coordinates using incorrect translation data, and these were corrected. For the most part, however, the older and newer locations are consistent. Differences between the two can be attributed both to the algorithmic improvements described above

and to more effective selection of source and background intervals that reduce the statistical errors in some cases.

5. THE STATISTICAL AND SYSTEMATIC BURST LOCATION ERRORS IN THE BATSE CATALOGS

5.1. Section Overview

In this section we discuss various properties of the statistical and systematic errors in the LOCBURST locations. We discuss some estimates of the differences between the 2B and post-2B catalog systematic errors. A more detailed multicomponent model of the current LOCBURST systematic error is presented in Briggs et al. (1998). We also discuss the intensity dependence of reduced χ^2 and put constraints on intensity dependence of the LOCBURST systematic error. The limitations of the catalog value of the statistical error are also discussed.

5.2. LOCBURST Statistical Error Calculation

The statistical error on the LOCBURST locations, referred to as σ in the BATSE burst catalogs, is calculated using the covariance matrix, C, for 2 angular degrees of freedom,

$$1 \ \sigma = \sqrt{\delta\theta(\delta\phi \cos \theta)} , \tag{1}$$

where θ is the source elevation angle, and ϕ is the source azimuthal angle, respectively, in GRO coordinates. Also,

$$\delta\theta = \sqrt{(\Delta\chi^2)C_{\theta\theta}} , \tag{2}$$

where $\Delta\chi^2 = 2.3$, because there are two parameters of interest (Press et al. 1986), and $C_{\theta\theta}$ is the diagonal element of the covariance matrix. $\delta\phi$ is defined in a similar fashion.

It should be noted here that this statistical error σ, as defined above in terms of the χ^2 increase for 2 degrees of freedom, represents the radius of the angular region containing 68% of the probability (the 68% confidence region) in the ideal case of circular error contours. The σ we have defined here, $\sigma_{LOCBURST}$, differs from $\sigma_{GAUSSIAN}$, (σ for a two-dimensional Gaussian) by the following factor,

$$\sigma_{GAUSSIAN} = 0.66 \times \sigma_{LOCBURST} . \tag{3}$$

When the actual location contours are noncircular, $\sigma_{LOCBURST}$ can differ significantly from the radius of the angular area containing 68% of the probability, as will be shown below.

5.3. Comparison of 2B and Post-2B Systematic Errors

For our LOCBURST location catalogs, a first-order estimate of the systematic error has been determined by comparison of LOCBURST locations with various sets of ILBs containing IPN (Hurley et al. 1996), WATCH (Gorosabel et al. 1996), COMPTEL (Kippen et al. 1998), and SAX (Heise et al. 1997) located bursts.

We calculate total errors for LOCBURST locations by evaluating the angular distance between the LOCBURST location and the ILB location for each ILB. Distributions of total errors and $\sigma_{LOCBURST}$ values are shown in Figure 10 for four different data sets, and representative error values for these distributions are shown in Table 1. The thick solid lines show the total error distributions, and the dotted lines show the $\sigma_{LOCBURST}$ distributions for each data set. The RMS value of the total error, $Total_{RMS}$, is shown in the first row of Table 1. $Total_{68\%}$, shown in the second row of Table
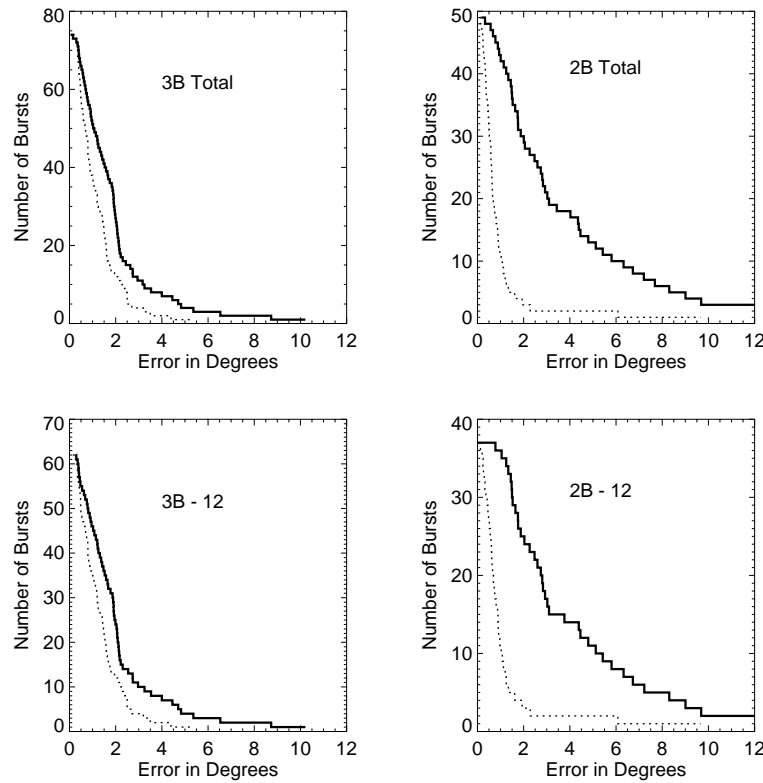
Fig. 10.—BATSE location error distributions calculated using ILB burst sets for the 3B and 2B versions of LOCBURST. Solid histograms, total errors; dotted histograms, LOCBURST statistical errors.

1, is the smallest value of the total error that, itself, is greater than 68% of the total error values. If the total error distribution were a two-dimensional Gaussian distribution, then $\mathrm{Total_{RMS}} = \sqrt{2} \times \sigma_{\mathrm{GAUSSIAN}} = 0.93 \times \mathrm{Total}_{68\%}$. Reasons why this does not hold for these data will be discussed below. $\mathrm{Stat_{ave}}$, in the third row of Table 1, is the average value of the $\sigma_{\mathrm{LOCBURST}}$ distribution. We use these values to produce two estimates for the 68% containment value for the BATSE systematic error using the following equations,

$$\mathrm{Sys^2_{RMS}} = (\mathrm{Total_{RMS}})^2 - (\mathrm{Stat_{ave}})^2 \, , \qquad (4)$$

$$\mathrm{Sys^2_{68\%}} = (\mathrm{Total}_{68\%})^2 - (\mathrm{Stat_{ave}})^2 \, . \qquad (5)$$

These systematic error estimates are given in the last two rows of Table 1.

The upper left panel of Figure 10, labeled 3B Total, shows the error distributions calculated for all ILBs using loca-

tions from the 3B LOCBURST algorithm. The value of $\mathrm{Sys}_{68\%}$ is consistent with the $1°\!.6$ reported in the 3B catalog. The upper right panel shows the same data for the 2B LOCBURST algorithm. Here $\mathrm{Sys}_{68\%}$ is $\sim 4°$, which is consistent with our earlier 2B systematic error estimates. The statistical errors are somewhat larger, on average, for the 3B data than for the 2B data. This difference is due to a more meticulous application of the high flux (greater than 50,000 counts s^{-1}) avoidance criterion to reduce the systematic response distortions due to dead-time correction inaccuracies.

As we mentioned above, we examined the locations of 12 of the earlier 1B bursts while implementing the improvements to the 3B location software. Results for the 2B and 3B LOCBURST data sets without these twelve bursts are shown in the lower right and left panels of Figure 10, respectively, labeled 3B-12 and 2B-12. The error estimates for these data sets are shown in Table 1 in the columns 3B-12

TABLE 1

2B AND 3B LOCBURST ERROR ESTIMATES IN DEGREES USING ILBS

Error	3B Total	3B-12	2B Total	2B-12	3B: Statistical Error ≤ 2.0
$\mathrm{Total_{RMS}}$ [a]	2.75	2.91	7.70	7.62	2.27
$\mathrm{Total}_{68\%}$ [b]	2.07	2.11	4.39	4.53	1.97
$\mathrm{Stat_{ave}}$ [c]	1.23	1.32	0.89	1.05	0.91
$\mathrm{Sys_{RMS}}$ [d]	2.07	2.59	7.64	7.55	2.07
$\mathrm{Sys}_{68\%}$ [e]	1.66	1.64	4.39	4.53	1.74

[a] Root mean square of the ILB to LOCBURST offsets (total error).
[b] Value of the total error containing 68% of the distribution of total errors.
[c] Average of the circular radius defining the 68% confidence region for the statistical errors on the locations, assuming circular error contours.
[d] Estimated systematic error using $\mathrm{Total_{RMS}}$.
[e] Estimated systematic error using $\mathrm{Total}_{68\%}$.

and 2B-12. These error analysis results are not changed appreciably by the presence or absence of these 12 bursts.

As we noted before, the values of Sys_{RMS} and $Total_{RMS}$ are significantly larger than the values of $Sys_{68\%}$ and $Total_{68\%}$, indicating non-Gaussian underlying distributions. This is partly due to the non-Gaussian nature of the statistical error distribution. The size of the difference, however, raises the possibility that the systematic error distribution itself is significantly non-Gaussian. The data in Figure 11 for 3B locations with ILBs and statistical errors less than 2° suggests the presence of a non-Gaussian tail to the systematic error distribution. As was mentioned above, a detailed analysis of the IPN arcs performed by Briggs et al. (1998) has demonstrated that a non-Gaussian error distribution is preferred by the data, using the catalog values of the LOCBURST location statistical errors.

5.4. Intensity-Dependent Properties of the LOCBURST Errors

In Table 2 we present estimates of the various location errors as a function of source intensity. At the bright end, we have the ILB burst locations. These LOCBURST locations have the smallest statistical errors, covering a range from 0° to 2°. To evaluate the systematics of lower intensity burst locations, short intervals from ILB bursts were used with lower intensities and statistical errors in the 2°–8° range. For the weakest burst estimates, fluctuations of Cygnus X-1 that triggered the BATSE burst mode with statistical errors in the 8°–14° range were used. These events have an average spectral index of 2.3 in the 50–300 keV range, making them suitable for studies of the intensity-dependent background subtraction systematics.

The top row of Table 1 contains the average value of the statistical error for the locations in each sample, $Stat_{ave}$, as defined above. The second row contains the standard error on $Stat_{ave}$, labeled $Stat_{err}$, to characterize the accuracy of the $Stat_{ave}$ values. In the third row the total error, $Total_{68\%}$, is given for each of these three location distributions.

TABLE 2
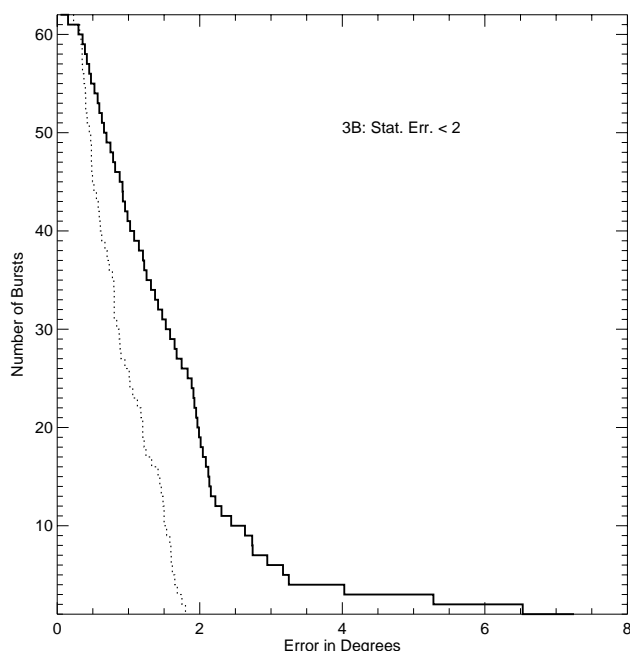LOCBURST Systematic Error Versus Intensity

Error	ILB Locations	ILB Sections	Cygnus X-1
$Stat_{ave}$ [a]	1.23	4.35	11.5
$Stat_{err}$ [b]	0.11	0.23	0.4
$Tot_{68\%}$ [c]	2.07	4.7	10.75
Sys [d]	1.66	1.75	0.0

[a] Average of the radius defining the 68% confidence region for the statistical errors on the locations.

[b] Standard error on $Stat_{ave}$.

[c] Value of the total error containing 68% of the distribution of total errors.

[d] Estimated systematic error.

In the last row, $Sys_{68\%}$, as defined above, is shown. There is no evidence in these data for a strong intensity-dependent systematic error that would be caused by significant and pervasive background subtraction systematics or any other mechanism. It is quite possible that background-subtraction systematics are present at some lower level; however, further studies will be required to evaluate such effects.

Another indicator of the intensity dependence of the LOCBURST systematic error is the reduced χ^2 for the final locations. Figure 12 shows the values of reduced χ^2 as a function of the catalog statistical error for four different classes of locations. The upper left panel shows the distribution for bursts located using CONT data from four detectors with 20 degrees of freedom. The data are consistent with a systematic error around 2° being convolved with the statistical error. The upper right panel, with 32 degrees of freedom, shows this effect somewhat more clearly. The lower left and right panels for locations using DISC data, with 5 and 9 degrees of freedom, respectively, have larger values of the reduced χ^2 than the CONT data, but this is to be expected given the smaller number of degrees of freedom.

5.5. Detailed Characterization of the LOCBURST Statistical Errors

As we described above, our contour map algorithm allows us to map out the actual χ^2 contour map for each burst location. Some comparisons between the contour map shapes (*solid contours*) and the catalog statistical errors (*dotted circles*) are shown in Figure 13. Another quantity is calculated numerically for these four bursts, using the χ^2 contour map data renormalized to an equal area grid and assigning an effective probability estimate to each grid point using $e^{-\Delta\chi^2/2}$. The circle marked with the dashed line represents the 68% probability radius using these data.

In the lower right panel all three of these contours match fairly well, as one would anticipate for a circularly symmetric error contour. Also shown in the panel is the aspect ratio, defined as the longest axis of the solid lined contour over the shortest axis, which is a first-order estimate of the ellipticity of the contour. Contours with smaller aspect ratios are more likely to have their errors represented accurately by the LOCBURST catalog value, although there is some variation to this correlation, as is shown by the contours in the lower panels of Figure 13. For larger aspect ratios, neither circular approximation to the error contour is particularly accurate, as is seen in the top two panels. In Figure 14 we show the contour aspect ratio distribution for the LOCBURST locations. Most aspect ratios are less than

3B: Stat. Err. < 2

Fig. 11.—BATSE location error distributions for 3B bursts with statistical errors less than 2°.
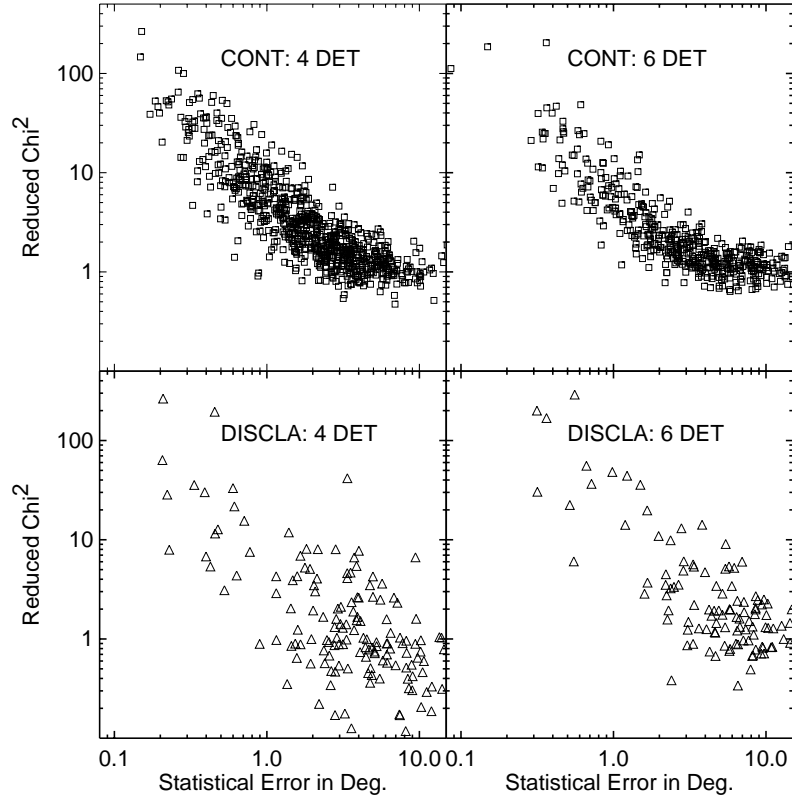
Fig. 12.—Reduced χ^2 vs. LOCBURST catalog statistical error for several data sets
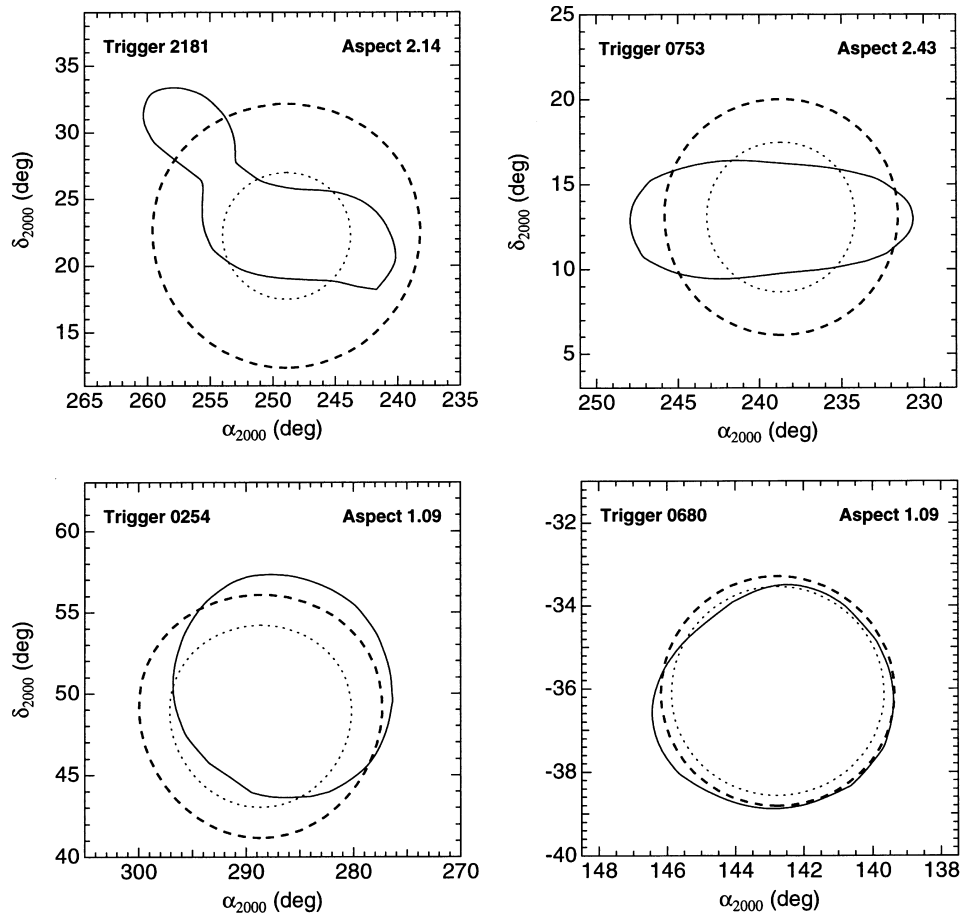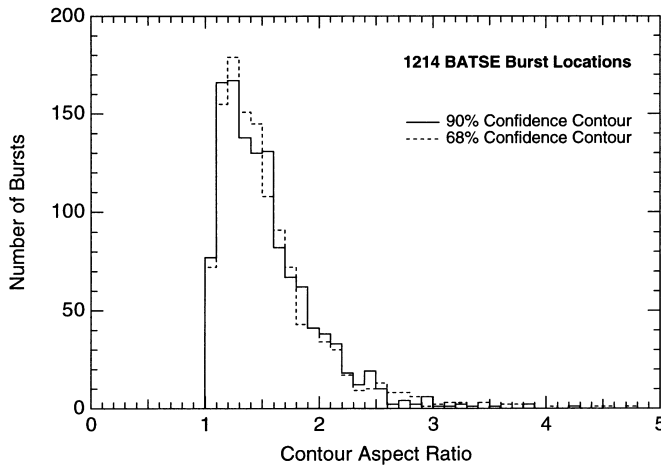

Fig. 13.—LOCBURST contour maps

FIG. 14.—Contour map aspect ratio

2, but the distribution has sizable width. Further studies of the LOCBURST statistical error contours and the systematic error will be performed in order to characterize them more fully.

6. FUTURE BURST LOCATION EFFORTS

Here we will summarize the aspects of burst detection of particular importance to the GRB location methodology for BATSE and potentially relevant to future GRB monitors. We will also describe future directions for LOCBURST improvements. The identification of GRB optical counterparts (Van Paradis 1997) has abruptly changed the requirements on future GRB location capabilities. The reader should therefore note that the direction of future burst location requirements could well change again.

We list here several properties of the GRB location process that contribute significantly to the complexity of the problem. Detectors with large fields of view are desirable to acquire the largest GRB population statistics possible. When the locations are calculated using such gamma-ray detectors, the detector response must be accurately modeled not only as a function of incident and detected energy, but also as a function of position in the sky.

In addition, the hardness of the average burst spectrum in the energy range used for burst location requires the collection of significant amounts of calibration data and the use of electromagnetic Monte Carlo simulations. Our experience with burst location using the BATSE instrument tells us that the hard spectra of GRBs in the 10 keV–1 MeV range make detailed modeling of the instrument response characteristics essential for accurate burst locations. The relatively hard GRB spectra make the off-diagonal component of the detector response due to high-energy photons depositing less than their total energy much more important than for softer sources.

Also, the broad range of average spectra exhibited by the members of the burst population requires a response model with a large number of dimensions to accurately realize the response of the instrument to bursts with significantly different spectra and temporal morphologies, since the systematic errors affecting the location accuracy of each type of burst vary substantially. For BATSE the spectral curvature modeling has an effect on the location accuracy for bursts that are extremely hard at lower energies and then break significantly at higher energies. However, there is only a

small fraction of the population where this modeling makes a difference.

For BATSE, the required complexity of the atmospheric scattering representation and the detailed level of its implementation results from the properties listed above. In fact, the hard spectrum alone would require simulations, but not the detailed and flexible level of the scattering representation present in the current analysis database. All-sky monitoring and the range of burst spectra require it. Any future instruments with significant exposure to Earth albedo will need a detailed model of atmospheric scattering as well.

There is also a good chance that new instruments will observe burst phenomena that were not recognized in the data sets obtained with the current instruments. Measurements of the duration, intensity, and spectral form of the shortest GRBs, for example, will be improved substantially in future missions. Shorter bursts have harder average spectra than longer bursts, and how this trend continues into unexplored regions of progressively shorter burst duration is unknown. It is not possible to predict with certainty what the characteristics of these events will be, and knowing precisely how to optimize the accuracy of a burst location algorithm may well require this knowledge. Therefore, anticipation of significant in-flight calibration by the scientific community would be prudent.

If resources permit, fully completed and flexibly constructed burst location algorithms should be ready before instrument launch. That way the process of in-flight algorithm optimization can be completed as quickly as possible, which will minimize the stress on both the instrument team and the scientific community when the analysis of the burst location data commences.

Recent developments in GRB observations, particularly the discovery of X-ray and optical transient counterparts to bursts, seem to indicate that GRB location accuracies for the burst detectors need to be no better than the fields of view of X-ray telescopes. Many current X-ray telescopes have fields of view on the order of 1°, and optical ground-based telescopes can be fitted with large CCD camera arrays, providing them with several-degree fields of view. Now fast burst locations that can be distributed to other instruments are of paramount importance.

To this end we have developed a rapid response version of LOCBURST that uses the data stream from BACCODINE as input to our fully developed location algorithm. Our goal is to produce burst locations for public distribution within half an hour and with an accuracy comparable with our best location algorithm. We also plan to improve the accuracy of the current BACCODINE algorithm that has been developed to produce locations within seconds of a burst trigger. Addition of the atmospheric scattering correction to this algorithm, for example, would significantly improve its accuracy. We will work to develop an atmospheric scattering representation optimized for speed.

7. SUMMARY

We have described here the rather arduous process required for the optimization of our burst location algorithm. The combination of the all-sky monitoring requirements and the varied characteristics of the bursts themselves contribute to the complexity of the problem. The BATSE 3B catalog burst location software is more accurate and thoroughly tested than the previous algorithms used to produce the burst locations. A number of

identifiable errors that affected the 2B catalog results were remedied in the 3B catalog. The procedures used to analyze the bursts were more rigorous and uniformly controlled than in any previous BATSE catalog. Our characterization of the location errors is more detailed than it has been for our previous catalogs. Further analyses will be performed to quantify the nature of the systematic errors more precisely. Our near-term future efforts will focus on increasing the speed with which we produce and distribute GRB locations.

REFERENCES

Briggs, M. S., et al. 1998, in preparation
Brock, M. N., et al. 1992, in AIP Conf. Proc. 265, Gamma-Ray Bursts, ed. W. S. Paciesas & G. J. Fishman (New York: AIP), 383
———. 1993, in AIP Conf. Proc. 280, *Compton Gamma Ray Observatory*, ed. N. Gehrels et al. (New York: AIP), 709
Fishman, G. J. et al. 1989, Proc. Gamma Ray Observatory Science Workshop, ed. W. N. Johnson (Greenbelt: Goddard Space Flight Center), 2
Gorosabel, J., et al. 1996, in AIP Conf. Proc. 384, Gamma-Ray Bursts: Third Huntsville Symp., ed. C. Kouvelitou (New York: AIP), 378
Heise, J., et al. 1997, IAU Circ. 6654
Horack, J. M., Meegan, C. A., Fishman, G. J., Wilson, R. B., Paciesas, W. S., Emslie, A. G., Pendleton, G. N., & Brock, M. N. 1993, ApJ, 413, 293
Hurley, K., et al. 1996, in AIP Conf. Proc. 384, Gamma-Ray Bursts: Third Huntsville Symp., ed. C. Kouvelitou (New York: AIP), 291

Kippen, R. M., et al. 1998, ApJ, 492, 246
Marsden, R. G., et al. 1996, Sky & Telescope, 3, 24
Meegan, C. A., et al. 1996, ApJS, 106, 65
Pendleton, G. N., et al. 1992, in NASA Conf. Pub. 3137, Proc. Compton Observatory Science Workshop, ed. C. R. Shrader (Washington DC: NASA), 47
Pendleton, G. N., et al. 1994, in AIP Conf. Proc. 304, Second Compton Symp., ed. C. E. Fitchel, N. Gehrels, & J. P. Norris (New York: AIP), 749
Pendleton, G. N., et al 1995b, ApJ, 439, 963
Pendleton, G. N., et al. 1995a, Nucl. Instrum. Methods A, 364, 567
Press, W. H., Flannery, B. P., Teukolsky, S. A., & Vetterling, W. T. 1986, Numerical Recipes (New York: Cambridge Univ.)
Van Paradijs, J., et al. 1997, Nature, 386, 686